JPE 17-1-16

https://doi.org/10.6113/JPE.2017.17.1.161
ISSN(Print): 1598-2092 / ISSN(Online): 2093-4718

Direct Torque Control of Five-leg Dual-PMSM Drive Systems for Fault-tolerant Purposes

Wei Wang†, Jinghao Zhang*, Ming Cheng*, and Ruiwu Cao**

†,*School of Electrical Engineering, Southeast University, Nanjing, China
**College of Automation Engineering, Nanjing University of Aeronautics and Astronautics, Nanjing, China

Abstract

To enhance the reliability of two-motor drive systems, this paper proposes an improved direct torque control (DTC) scheme (P-DTC) for five-leg dual-PMSM drive systems. First, the topology of a five-leg dual-PMSM drive system is illustrated. To clarify the analysis of the P-DTC, the standard DTC scheme for three-phase drive systems is presented. The operation of a five-leg dual-PMSM drive system is classified into three situations according to the definitions of the switching-vector unions. Compared with the existing DTC scheme (R-DTC), the P-DTC can minimize the replacement of active switching-vectors to zero switching-vectors. When this replacement cannot be avoided, the P-DTC uses a proposed master-slave selection principle to minimize the system error. Comparing with the R-DTC, the P-DTC has lower torque ripples, a wider speed range and a faster torque increasing response. Experiments have been carried out in the coupling and independent modes, and the effectiveness of the P-DTC is verified by the obtained results

Key words: Direct torque control, Fault tolerance, Five-leg VSI, PMSM

I. INTRODUCTION

Due to its high efficiency and high power-density, the permanent-magnet synchronous machine (PMSM) has received a lot of attention, and it has become a competitive candidate for traction motors [1]-[6]. In some traction applications, one PMSM cannot provide enough torque. Therefore, several PMSMs need to operate together. It is known that the torque of a PMSM is mainly determined by the power angle. However, these co-operated PMSMs cannot always remain at the same speed. Therefore, one three-leg voltage-source-inverter (VSI) usually controls one three-phase PMSM [7]. Hence, more power switching devices are used in multi-PMSM drives, which results in more component faults. According to [8], the failure rate of power switching devices contributes more than 50% of the remaining component faults. Once a power switching device in a VSI fails, the system performances may be significantly degraded and the system operation may have to be halted. To enhance the system reliability, fault-tolerant operation of multi-PMSM drives is usually necessary. As a precondition to fault-tolerant operation, the faults of the power switching devices must be detected. So far, many fault-detection methods for power switching devices have been proposed [9]-[17]. Once the faults of the power switching devices are detected, the fault system enters the fault-tolerant operation.

For a dual-motor drive system, two three-leg VSIs are usually required under normal conditions, which is defined as a six-leg dual-motor drive system in this paper. Recently, five-leg dual-motor drive systems have received a lot of attention [18]-[26], where two three-phase motors are controlled by one five-leg VSI. Compared with six-leg dual-motor drive system the five-leg dual-motor drive systems can save one leg. Therefore, the latter can be treated as a fault-tolerant topology for the former. It should be emphasized that five-leg dual-motor drive systems have lower dc bus voltage utilization. In the worst possible case, the dc bus voltage utilization of a five-leg dual-motor drive system can be halved [18].

So far, many control methods have been proposed for the five-leg dual-motor drive system and they can be classified into two types: pulse-width-modulation (PWM)-based and

Manuscript received Aug. 25, 2016; accepted Oct. 19, 2016
Recommended for publication by Associate Editor Kwang-Woon Lee.
†Corresponding Author: wangwei1986@seu.edu.cn
Tel: +86-25-83794152, Fax: +86-25-83791696, Southeast University
*School of Electrical Engineering, Southeast University, China
**College of Automation Engineering, Nanjing University of Aeronautics and Astronautics, China

switch-based. The PWM-based control methods have one or more PWM modulators, while the switch-based control methods have no PWM modulators. In [18]-[21], several PWM-based control methods were proposed, and any reference voltage can be theoretically realized in the linear modulation region. However, this is difficult for the switch-based control methods. As analyzed in [22], implementation troubles usually exist in switch-based control methods. To solve these implementation problems, some switch-based control methods have been proposed [23]-[26].

In [23], a specific coding yields an inversion table which represents the relationship between the modulation function and the switching function. The modulation function is generated by the reference phase-phase voltage according to the PWM strategy. The corresponding switching function is found from the look-up table by the modulation function. However, sometimes the modulation function does not have an equivalent switching function. In this situation, the previous switching function is taken as a replacement but no theoretical basis is provided.

In [22], a dual-level hysteresis current control (HCC) is proposed for five-leg dual-motor drive systems. In the dual-level HCC, six phase-switch-states are determined by the standard three-phase HCC. The coupling phase with the largest absolute value of the phase current error is determined as the master coupling phase, and the leg-switch-state of the common leg is set as the phase-switch-state of the master coupling phase. Additionally, the phase-switch-states of four individual phases are directly assigned to four individual legs. As a result, the implementation trouble can be successfully solved.

Considering the nonlinear tuning of conventional synchronous current regulators, the finite-control-set model predictive control (FCS-MPC) was designed for five-leg dual-motor drive systems [24], [25]. The computational burden is reduced by using a reduced set of voltage vectors, and multi-object control can be realized. However, the FCS-MPC requires more machine parameters, which reduces the system robustness. In addition, the computational speed of the process chip should be fast enough to execute the FCS-MPC.

It is known that direct torque control (DTC) is widely used for motor drives [27], [28]. In addition, the standard DTC (S-DTC) contains one or more look-up tables. S-DTC has been applied to five-leg dual-motor drives [26], where a pulse generator is used to separate two motors. The pulse generator has two discrete values (0 and 1) that are randomly generated. Therefore, this DTC scheme is denoted as random DTC (R-DTC) in this paper. The implementation trouble is solved according to the following method: if the pulse amplitude is 1, the original switching-vector of the first motor is replaced by a zero vector; otherwise, the original switching-vector of the second motor is replaced by a zero vector. However, the effectiveness of the R-DTC has only been verified by simulation results, and no detailed analyses have been carried out. It has been determined that the R-DTC may result in higher torque ripples, a longer rising time of the torque response and a narrower speed range, which will be analyzed in this paper.

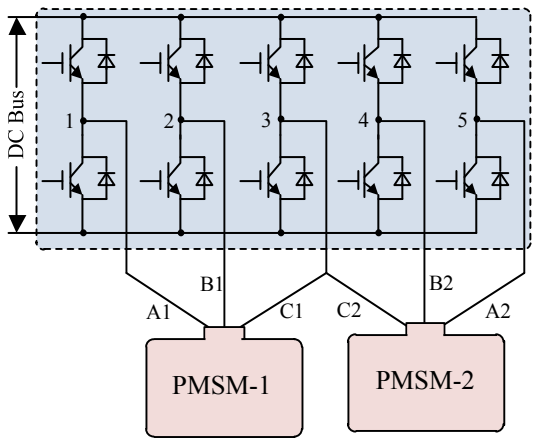

Fig. 1. Five-leg dual-PMSM drive system.

Based on the above-mentioned considerations, an improved DTC scheme is proposed in this paper for five-leg dual-PMSM drive systems. This scheme is denoted as P-DTC. A detailed theoretical analysis and experimental validation are provided. This paper is organized as follows. The five-leg dual-motor drive system is defined in Section II. The S-DTC and P-DTC are presented in Section III and Section IV, respectively. Their performances are theoretically compared in Section V. These comparisons are verified by experiments in Section VI. Finally, some conclusions are drawn in Section VII.

II. Five-leg Dual-PMSM Drive System

Fig. 1 shows a five-leg dual-PMSM drive system, in which two surface-mounted three-phase PMSMs (PMSM-1 and PMSM-2) are controlled by one five-leg VSI. The three phases of PMSM-1 are referred to as Phase-A1, Phase-B1 and Phase-C1, while the three phases of PMSM-2 are referred to as Phase-A2, Phase-B2 and Phase-C2. Four individual phases (Phase-A1, Phase-B1, Phase-A2 and Phase-B2) are connected to four individual legs (leg-1, leg-2, leg-5 and leg-4), respectively. The common leg (leg-3) is shared by two coupling phases (Phase-C1 and Phase-C2).

III. S-DTC

In order to clarify the operation principles of the P-DTC, the basic concepts of the S-DTC are briefly described as follows. A three-leg drive system is illustrated in Fig. 2, where the positive directions of the phase currents are defined as the arrow directions.

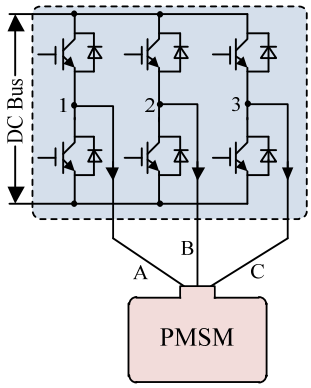

Fig. 2. Three-leg PMSM drive system.

The PMSM can be modeled as follows:

$$\boldsymbol{u}_s = R_s \boldsymbol{i}_s + \frac{d\boldsymbol{\psi}_s}{dt} \tag{1}$$

$$T_e = 1.5 p_n (\psi_\alpha i_\beta - \psi_\beta i_\alpha) \tag{2}$$

with

$$\boldsymbol{u}_s = \begin{bmatrix} u_\alpha \\ u_\beta \end{bmatrix}, \boldsymbol{i}_s = \begin{bmatrix} i_\alpha \\ i_\beta \end{bmatrix}, \boldsymbol{\psi}_s = \begin{bmatrix} \psi_\alpha \\ \psi_\beta \end{bmatrix}$$

where R_s is the stator resistance, T_e is the electromagnetic torque, p_n refers to the pole pairs, ψ_α and ψ_β are the α-axis and β-axis stator fluxes, u_α and u_β are the α-axis and β-axis stator voltages, and i_α and i_β are the α-axis and β-axis stator currents.

By modifying (1), ψ_α and ψ_β can be calculated as follows:

$$\boldsymbol{\psi}_s = \int (\boldsymbol{u}_s - R_s \boldsymbol{i}_s) dt + \boldsymbol{\psi}_{f0} \tag{3}$$

with

$$\boldsymbol{\psi}_{f0} = \begin{bmatrix} \psi_{f\alpha} \\ \psi_{f\beta} \end{bmatrix} = \begin{bmatrix} \psi_f \cos\theta_{init} \\ \psi_f \sin\theta_{init} \end{bmatrix}$$

where ψ_f is the permanent-magnet flux, and θ_{init} is the initial rotor position. u_α, u_β and i_α, i_β can be obtained by a coordinate transformation from the three-phase stationary coordinate abc to the two-axis stationary coordinate $\alpha\beta$ by aligning the α-axis along the phase-A of the stator:

$$\begin{cases} \begin{bmatrix} i_\alpha & i_\beta \end{bmatrix}^T = T_{2/3} \begin{bmatrix} i_a & i_b & i_c \end{bmatrix}^T \\ \begin{bmatrix} u_\alpha & u_\beta \end{bmatrix}^T = \boldsymbol{T}_{2/3} u_{dc} \begin{bmatrix} k_a & k_b & k_c \end{bmatrix}^T \end{cases} \tag{4}$$

with

$$\boldsymbol{T}_{2/3} = \frac{1}{3} \begin{bmatrix} 2 & -1 & -1 \\ 0 & \sqrt{3} & -\sqrt{3} \end{bmatrix} \tag{5}$$

where u_{dc} is the measured DC-link voltage; k_a, k_b, and k_c are the phase-switch-states (PSSs); and i_a, i_b and i_c are the measured phase-A, phase-B and phase-C currents. The stator flux ψ_m and its phase angle δ can be calculated as follows:

$$\boldsymbol{\psi}_s = \psi_m \angle \delta \tag{6}$$

The flux state ε_ψ and the torque state ε_T are generated by two hysteresis comparators:

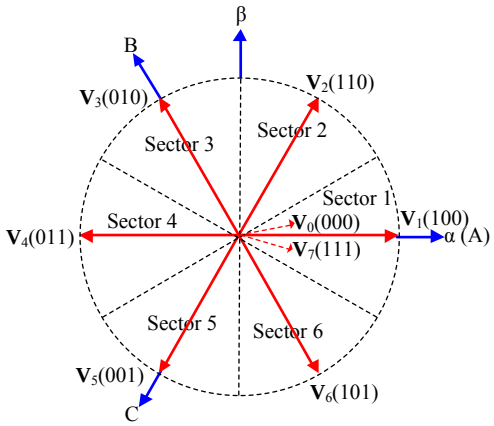

Fig. 3. Distribution diagram of space voltages and flux sectors of S-DTC.

$$\varepsilon_\psi = \begin{cases} 1, & if \quad \Delta\psi_m > H_\psi / 2; \\ 0, & if \quad \Delta\psi_m < -H_\psi / 2. \end{cases} (\Delta\psi_m = \psi_m^* - \psi_m) \tag{7}$$

and

$$\varepsilon_T = \begin{cases} 1, & if \quad \Delta T_e > H_T / 2; \\ 0, & if \quad \Delta T_e < -H_T / 2. \end{cases} (\Delta T_e = T_e^* - T_e) \tag{8}$$

where $\Delta\psi_m$ and ΔT_e are the errors of the stator flux and torque, respectively; ψ_m^* and T_e^* are the references of the stator flux and electromagnetic torque, respectively; and H_ψ and H_T are the hysteresis bands of stator flux and torque comparators, respectively.

Flux sector N is determined by:

$$\pi(2N-3)/6 <= \delta < \pi(2N-1)/6, N = 1,2,3,4,5,6 \tag{9}$$

The distribution of flux sectors is illustrated in Fig. 3, and the boundaries of the flux sectors are given by the dashed line.

The eight space voltages, including six active vectors ($\mathbf{V}_1$-$\mathbf{V}_6$) and two zero vectors ($\mathbf{V}_0$, $\mathbf{V}_7$), are labeled with the PSSs (k_a, k_b and k_c) and illustrated in Fig. 3. The selection principles of the switching-vectors are listed in Table I. Here, the zero vectors are used to reduce the torque, and they are determined according to the minimization principle of the switching amount. For example, if the switching-vector in the previous switching period is 101 and a zero switching-vector is required in the current switching period, $\mathbf{V}_7$ is selected since only one switching action occurs.

Fig. 4 shows a block diagram of the S-DTC. Because the phase amount is equal to the leg amount, the PSSs can be directly assigned to three legs:

$$\begin{cases} s_1 = k_a \\ s_2 = k_b \\ s_3 = k_c \end{cases} \tag{10}$$

where s_i (i=1, 2, 3; s=1 means the switch is closed, and s=0 means the switch is open) is the leg-switching-state (LSS) of leg-i. Hence, the control targets ψ_m^* and T_e^* can be achieved by controlling the three-leg VSI.

TABLE I
SELECTION PRINCIPLES OF SWITCHING-VECTORS FOR S-DTC

	ε_T=1		ε_T=0
	ε_ψ=1	ε_ψ=0	
Sector 1	$\mathbf{V}_2$	$\mathbf{V}_3$	$\mathbf{V}_0$ or $\mathbf{V}_7$
Sector 2	$\mathbf{V}_3$	$\mathbf{V}_4$	
Sector 3	$\mathbf{V}_4$	$\mathbf{V}_5$	
Sector 4	$\mathbf{V}_5$	$\mathbf{V}_6$	
Sector 5	$\mathbf{V}_6$	$\mathbf{V}_1$	
Sector 6	$\mathbf{V}_1$	$\mathbf{V}_2$	

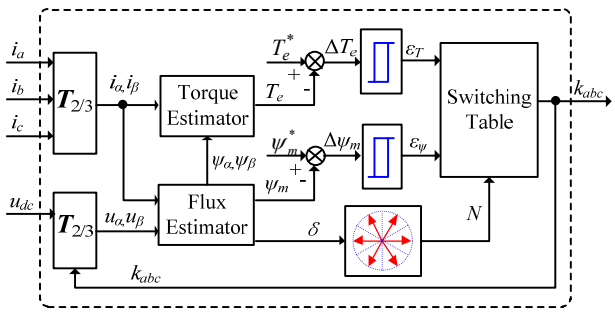

Fig. 4. Control diagram of S-DTC.

IV. P-DTC

Without special declarations, the subscripts "1" and "2" indicate PMSM-1 and PMSM-2 respectively in this paper. First, the PSSs k_{abc1} and k_{abc2} are determined by the S-DTC. Referring to Fig. 1, the P-DTC is proposed for dual-PMSM drive systems in this section.

A. Existing Problem

According to Fig. 1, five LSSs are required. However, there are six PSSs. If k_{c1} is equal to k_{c2}, both k_{c1} and k_{c2} can be implemented at the same time by setting s_3 as k_{c1} or k_{c2}. However, k_{c1} may be different from k_{c2}, which results in an implementation problem since s_3 cannot be changed during one switching period. The task of the P-DTC is to solve this implementation problem.

B. Analysis of Different Situations

To clarify the analysis, the switching-vector union **U** is defined as follows:

$$\mathbf{U}_{10i+j} = (\mathbf{V}_i, \mathbf{V}_j), i = 0...7, j = 0...7 \quad (11)$$

Obviously, there are 64 different switching-vector unions in total, and they are listed in TABLE II. These switching-vector unions are classified into three situations:

1) Situation-I: k_{c1} is equal to k_{c2}.

2) Situation-II: k_{c1} is different from k_{c2}, and either k_{abc1} or k_{abc2} is the zero switching-vector.

3) Situation-III: k_{c1} is different from k_{c2}, and both k_{abc1} and k_{abc2} are active switching-vectors.

Situation-I has 32 switching-vector unions, and there are no implementation problems since k_{c1} is equal to k_{c2}.

TABLE II
CLASSIFICATION OF SWITCHING-VECTOR UNIONS

$\mathbf{V}_i$ \ $\mathbf{V}_j$	0	1	2	3	4	5	6	7
0	I	I	I	I	II	II	II	II
1	I	I	I	I	III	III	III	II
2	I	I	I	I	III	III	III	II
3	I	I	I	I	III	III	III	II
4	II	III	III	III	I	I	I	I
5	II	III	III	III	I	I	I	I
6	II	III	III	III	I	I	I	I
7	II	II	II	II	I	I	I	I

Situation-II has 14 switching-vector unions, in which k_{abc1} or k_{abc2} is the zero switching-vector. It is known that there are two different zero vectors: $\mathbf{V}_0$ and $\mathbf{V}_7$. According to the operation principles of the S-DTC, a zero switching-vector is determined from two candidates ($\mathbf{V}_0$ and $\mathbf{V}_7$) to minimize the switching amount. By ignoring the stator resistance and switching amount, $\mathbf{V}_0$ and $\mathbf{V}_7$ have the same control effects. Therefore, one zero switching-vector can be replaced by another one. For example, if the two selected switching-vectors are 110 (k_{abc1}) and 111 (k_{abc2}), then k_{abc2} can be replaced by $\mathbf{V}_0$(000). Hence, k_{c2} becomes the same as k_{c1}. On the one hand, the implementation problem is successfully solved. On the other hand, there is no performance loss.

Situation-III has 18 switching-vector unions. In Situation-III, both of the selected switching-vectors are active and there is no zero switching-vector. Obviously, at least one selected active switching-vector must be modified in order to solve the implementation problem. This means that the control targets of the two PMSMs cannot be satisfied at the same moment. Therefore, the performance of the corresponding PMSM will be affected. The modification principles of the selected switching-vectors for Situation-III are introduced in the next subsection.

C. Master-Slave Selection Principle

If modification cannot be avoided, only one selected switching-vector is modified in Situation-III to reduce the performance degradation. To evaluate the performance degradation, the system errors of two PMSMs are defined as follows:

$$\begin{cases} f_{err1} = (\dfrac{\Delta T_{e1}}{T_{rated1}})^2 + \lambda(\dfrac{\Delta \psi_{m1}}{\psi_{f1}})^2 \\ f_{err2} = (\dfrac{\Delta T_{e2}}{T_{rated2}})^2 + \lambda(\dfrac{\Delta \psi_{m2}}{\psi_{f2}})^2 \end{cases} \quad (12)$$

where λ is a coefficient constant; f_{err1} and f_{err2} are the system errors of PMSM-1 and PMSM-2; T_{rated1} and T_{rated2} are the rated torques of PMSM-1 and PMSM-2; and ψ_{f1} and ψ_{f2} are the permanent-magnet fluxes of PMSM-1 and PMSM-2. It can be seen from (12) that the system errors are relative

values, which consider the parameter differences between PMSM-1 and PMSM-2. In other words, the P-DTC can be used for two PMSMs that are the same, or two PMSMs that are different.

The PMSM with the larger system error is defined as the master PMSM, and its selected switching-vector is defined as the master selected switching-vector. Similarly, the PMSM with the smaller system error is defined as the slave PMSM, and its selected switching-vector is defined the slave selected switching-vector. According to TABLE I, the S-DTC attempts to reduce the absolute torque error $|\Delta T_e|$ and the absolute flux error $|\Delta\psi_m|$ by selecting a proper switching-vector. Referring to (12), the control target of the S-DTC can also be represented to reduce the system error. If the selected switching-vector is not implemented, the corresponding system error may be increased since either $|\Delta T_e|$ or $|\Delta\psi_m|$ is enlarged. To minimize the maximum system error, the slave selected switching-vector is modified. Obviously, the performances of the master PMSM remain unchanged while the performances of the slave PMSM are degraded.

Ignoring the stator resistance, the stator flux vector $\boldsymbol{\psi}_s$ remains unchanged if one zero switching-vector is implemented. According to TABLE I, the active switching-vector is only selected when ΔT_e is positive. If the selected switching-vector is replaced by a zero vector, $|\Delta T_e|$ is further enlarged and the system error is increased. However, once the system error of the slave PMSM becomes larger than that of the master PMSM, their roles are immediately exchanged. Hence, one PMSM cannot always be the slave and the maximum system error can be limited. Based on the above-mentioned consideration, the selected active switching-vector is replaced by a zero switching-vector when a modification is required.

D. Control Method

Based on the above-mentioned analysis, the P-DTC is proposed in this subsection and its control flowchart is illustrated in Fig. 5. First, k_{abc1} and k_{abc2} are determined by S-DTC. Then the LSSs are determined by the following steps.

Step 1: if k_{c1} is equal to k_{c2}, the LSSs are determined by (13). Then, go to Step 5.

Step 2: if k_{abc1} is a zero switching-vector, the LSSs are determined by (14). Then, go to Step 5.

Step 3: if k_{abc2} is a zero switching-vector, the LSSs are determined by (15). Then, go to Step 5.

Step 4: if f_{err1} is not smaller than f_{err2}, the LSSs are determined by (15); otherwise, the LSSs are determined by (14).

Step 5: the LSSs are output to control the five-leg VSI.

$$s_1 = k_{a1}, s_2 = k_{b1}, s_3 = k_{c1}, s_4 = k_{b2}, s_5 = k_{a2} \quad (13)$$

$$s_1 = k_{c2}, s_2 = k_{c2}, s_3 = k_{c2}, s_4 = k_{b2}, s_5 = k_{a2} \quad (14)$$

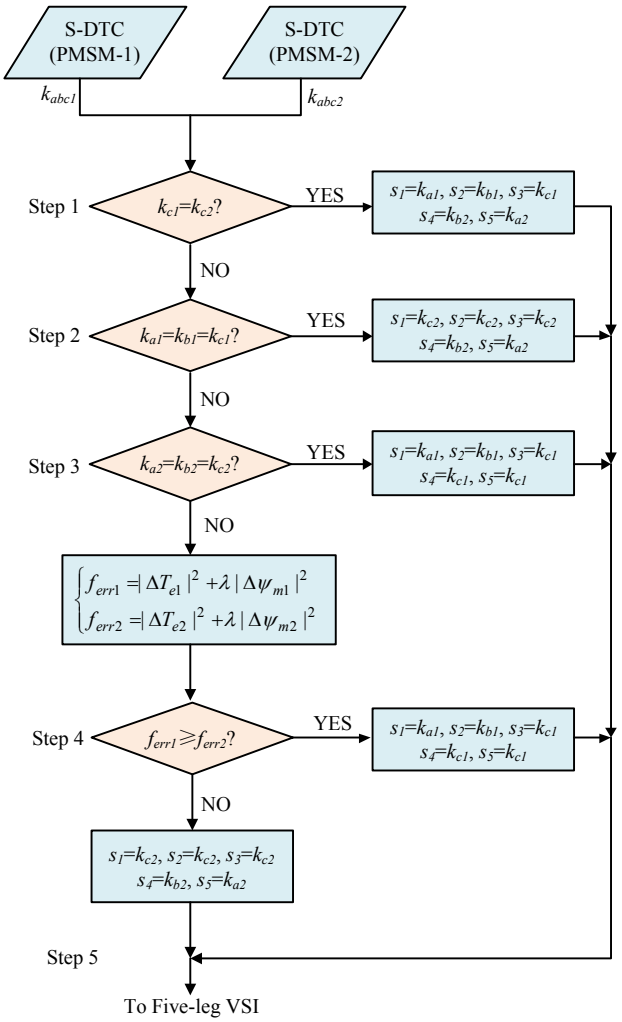

Fig. 5. Control flowchart of P-DTC.

$$s_1 = k_{a1}, s_2 = k_{b1}, s_3 = k_{c1}, s_4 = k_{c1}, s_5 = k_{c1} \quad (15)$$

Obviously, the P-DTC does not depend on a specific phase. Therefore, the P-DTC is generic for five-leg dual-PMSM drive systems and no special modifications are required. For example, the P-DTC can be directly employed if leg-3 is shared by Phase-C1 and Phase-A2.

E. Switching Loss

Switching loss is an important issue in general DTC, which is mainly influenced by the amount of switching actions. It is known that the P-DTC is proposed on the basis of the S-DTC. Therefore, the switching action of the P-DTC is compared with that of the S-DTC. In this subsection, both the S-DTC and the P-DTC are used to control two PMSMs that are the same. For dual-PMSM drive systems, the P-DTC requires one five-leg VSI while the S-DTC requires two three-leg VSIs. For a fair comparison, the switching loss of the common leg (leg-3) caused by one switching action is assumed to be twice that of one individual leg. As a result, the five-leg VSI can be considered as two special three-leg VSIs.

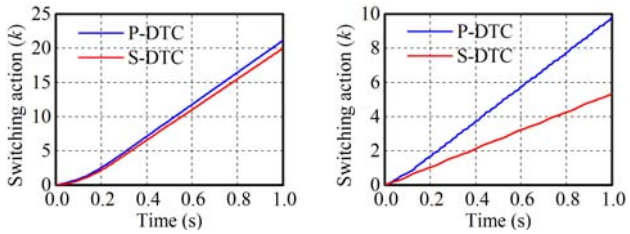

Fig. 6. Switching action comparison between P-DTC and S-DTC. (a) PMSM-1 with 300 r/min; (b) PMSM-2 with 50 r/min.

In Situation-I, both k_{abc1} and k_{abc2} can be directly implemented. Therefore, the P-DTC and the S-DTC have the same switching actions in this situation.

In Situation-II, one zero vector is changed to another zero vector. It is assumed that $k_{abc1}(n)$ is 000. According to the P-DTC, $k_{abc1}(n)$ should be changed to 111. According to the selection principle of the switching table in the S-DTC, the previous switching-vector $k_{abc1}(n\text{-}1)$ should be 000, 001, 010 or 100. Compared with the S-DTC, one or three switching actions are increased in each switching period by using the P-DTC.

In Situation-III, one active switching-vector is replaced by one zero vector by using the P-DTC. According to the selecting principle of the switching table in the S-DTC, the previous switching-vector of an active switching-vector can be any switching-vector. Therefore, the switching action can be increased or decreased by using the P-DTC. From the viewpoint of statistics, the P-DTC and the S-DTC have same switching actions in this situation.

According to the above-mentioned analysis, the switching actions are increased by using the P-DTC during the whole operation range. To verify this analysis, a simulation is carried out and the simulation results are illustrated in Fig. 6. In the simulation, the speed of PMSM-1 is 300 r/min while the speed of PMSM-2 is 50 r/min. It can be clearly seen in Fig. 6 that the P-DTC results in more switching actions. The increase in the switching actions has a greater significance to PMSM-2 since its speed is lower. The reason is that PMSM-2 requires more zero vectors according to the S-DTC. When the drive system comes into Situation-II, it is more likely that k_{abc2} is one zero vector and is changed to another zero vector according to the P-DTC. As a result, more switching actions occur.

V. Comparison Analysis

The P-DTC and the R-DTC are compared in this section.

A. R-DTC

To clarify the comparison analysis, the R-DTC is briefly presented and its control flowchart is illustrated in Fig. 7. In the R-DTC, k_{abc1} and k_{abc2} are also determined by the S-DTC, and the LSSs are determined by following steps.

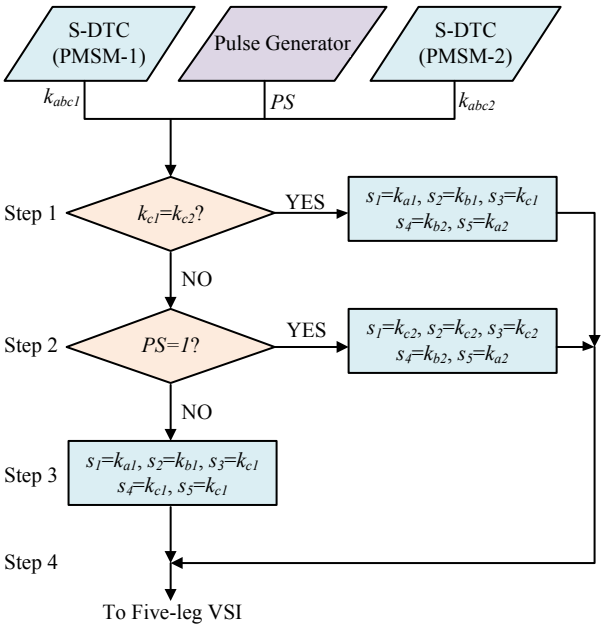

Fig. 7. Control flowchart of R-DTC.

Step 1: if k_{c1} is equal k_{c2}, the LSSs are determined by (13). Then, go to Step 4.

Step 2: if the random generated pulse *PS* is 1, the LSSs are determined by (14). Then, go to Step 4.

Step 3: if the random generated pulse *PS* is 0, the LSSs are determined by (15).

Step 4: the LSSs are output to control the five-leg VSI.

B. Torque and Flux Ripples

The P-DTC and the R-DTC have different control strategies in Situation-II and Situation-III.

In Situation-II, the P-DTC replaces one zero switching-vector with another zero switching-vector, and no performance degradation occurs. However, the R-DTC replaces one switching-vector with one zero switching-vector, and the replaced switching-vector may be an active one. As analyzed in Section IV, such a replacement results in larger torque ripples while the flux ripples remain unchanged.

In Situation-III, both the P-DTC and the R-DTC replace one active switching-vector with one zero switching-vector. Therefore, they can maintain the same level of flux ripple. However, their torque ripples are enlarged. Since the master-slave selection principle is employed, the maximum system error can be reduced in the P-DTC. Because the flux ripples are unchanged, the torque ripples are reduced in the P-DTC according to (12).

Generally speaking, the P-DTC achieves smaller torque ripples while both the P-DTC and the R-DTC have same level of flux ripple.

C. Speed Range

Since PMSMs belong to synchronous machines, the mechanical rotor and stator flux should have the same

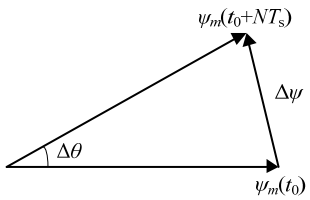

Fig. 8. Response procedure of stator flux of DTC.

rotational speed. Fig. 8 illustrates the response procedure of the stator flux, where the amplitude of the stator flux is changed from $\psi_m(t_0)$ to $\psi_m(t_0+N\cdot T_s)$ with a flux change of $\Delta\psi_m$. Correspondingly, the phase angle of the stator flux is changed by $\Delta\theta$ and the duration of $\Delta\psi_m$ is $N\cdot T_s$ (T_s is the sampling period, and N is the number of the sampling period). To simplify the analysis, both $\psi_m(t_0)$ and $\psi_m(t_0+N\cdot T_s)$ are supposed to match reference ψ_m^* well, that is:

$$\psi_m(t_0)=\psi_m(t_0+N\cdot T_s)=\psi_m^* \tag{16}$$

Because this is very small, $\Delta\theta$ can be given by:

$$\Delta\theta \approx \Delta\psi_m/\psi_m^* \tag{17}$$

The average rotational speed $\overline{\omega}$ of the stator flux can be computed by:

$$\overline{\omega}=\Delta\theta/(N\cdot T_s) \tag{18}$$

Obviously, the N sampling periods can consist of N_a zero switching-vectors and N_b (N_b=N-N_a) active switching-vectors. Because the zero switching-vector has no influence on the change of the stator flux, (18) can be rewritten as:

$$\overline{\omega}=\Delta\theta/(\eta\cdot N\cdot T_s) \tag{19}$$

where η is the ratio of the active switching-vector, η=N_b/N. Because more active switching-vectors are replaced by zero switching-vectors in the R-DTC, the value of η in the R-DTC is smaller than that in the P-DTC. Therefore, the P-DTC has a wider speed range.

D. Torque Response

According to TABLE I, the torque is reduced by selecting a zero switching-vector and it is increased by selecting a proper active switching-vector. Whether in the P-DTC or the R-DTC, it is impossible to replace a zero switching-vector with an active switching-vector. Therefore, both the P-DTC and the R-DTC have the same falling time for the torque response. As analyzed in Section V-C, more active switching-vectors are replaced by zero vectors in the R-DTC. Hence, the rising time of the torque response is lengthened in the R-DTC.

VI. Experimental Validation

The performances of the P-DTC and the R-DTC are compared in this section. Two operation modes are verified. The first operation mode is the coupling mode, in which two

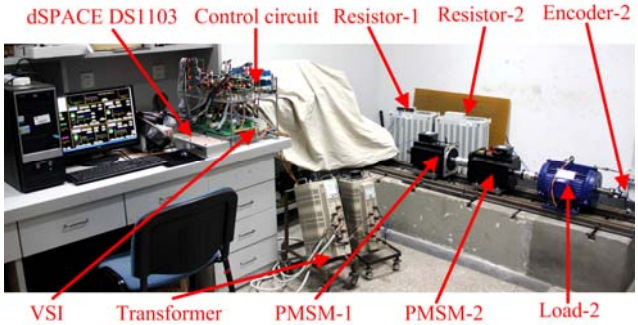

Fig. 9. Experiment platform for coupling mode.

TABLE III
Parameters of PMSM

Parameter	Value
Rated power	5.5 kW
Rated line voltage	380 V
Rated phase current	11 A
Rated speed	1500 rpm
Stator resistance R_s	0.625 Ω
Stator inductance L_s	8.5 mH
Permanent magnet flux ψ_{PM}	0.442 Wb
Number of pole pairs P_n	4

PMSMs share one common shaft and their speeds are always the same. The second operation mode is the independent mode, in which two PMSMs can be controlled independently and their speeds can be different. In the following experiments, the torque and the flux are calculated by (2) and (3), respectively.

A. Coupling Mode

To compare the performances of the P-DTC and the R-DTC in the coupling mode, an experimental platform was developed in the lab, as shown in Fig. 9. PMSM-1 and PMSM-2 are connected by a 5.5 kW load PMSM with an encoder of 1024 pulses per revolution. The load is realized by the close-loop torque control of the load PMSM using the field oriented control (FOC). The parameters of PMSM-1 and PMSM-2 are listed in TABLE III. A five-leg VSI is used to control PMSM-1 and PMSM-2. Braking resistors are installed for over-voltage protection.

The control program is implemented in a dSPACE DS1103 controller. The inputs for the dSPACE DS1103 controller are the measured phase currents and the feedback signal of the encoder. The switch states for the five-leg VSI are generated by the dSPACE DS1103 controller. A personal computer is employed for editing the control program and commanding the dSPACE DS1103 controller. The sampling frequency is 20 kHz.

To check the steady-state performances in the coupling mode, Experiment-1 is carried out and its experimental conditions are set as follows: a) the dc bus voltage is 400 V; b) the reference speed is set as 600 r/min; c) the total load is set

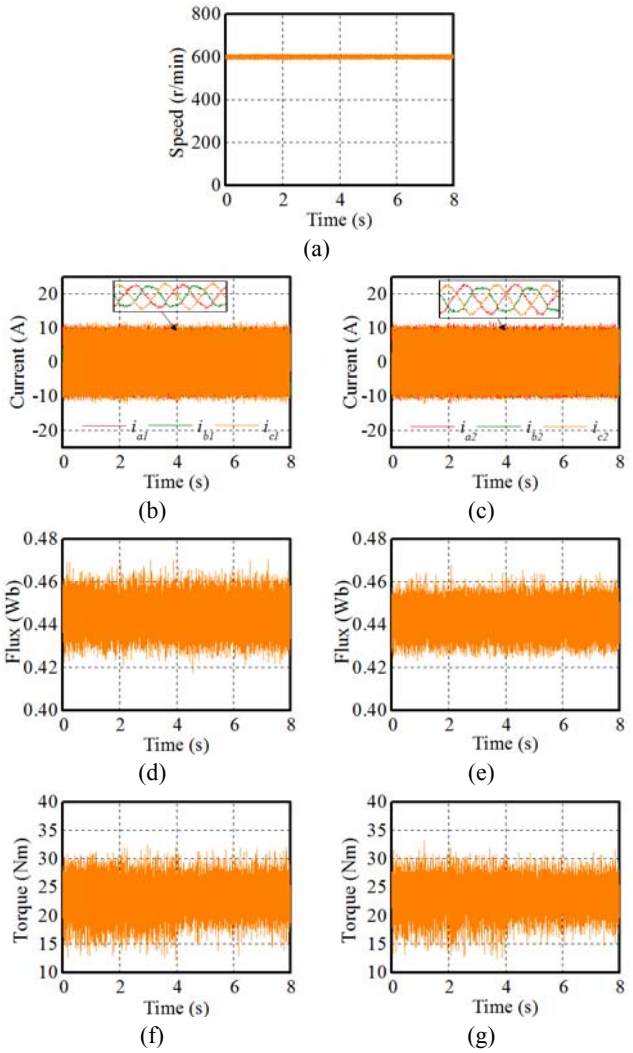

Fig. 10. Steady-state experimental results of coupling mode from R-DTC to P-DTC switching at t=0.4s. (a) Speed, (b) phase currents of PMSM-1, (c) phase currents of PMSM-2, (d) stator flux of PMSM-1, (e) stator flux of PMSM-2, (f) torque of PMSM-1, (g) torque of PMSM-2.

as 40 Nm; and d) the control method is switched from the R-DTC to the P-DTC at t=4s. Fig. 10 shows the experimental results of Experiment-1. It can be seen in Fig. 10 that the flux ripples remain unchanged while the torque ripples are reduced. This verifies the theoretical analysis of Subsection V-B.

To check the maximum speed in the coupling mode, Experiment-2 is carried out and its experimental conditions are set as follows: a) for safety purpose, the dc bus voltage is set as 100 V; b) the reference speed is set as 1000 r/min; and c) the total load is set as 40 Nm. Obviously, the speed target of 1000 r/min cannot be reached with a 100 V dc bus voltage. The corresponding experimental results are illustrated in Fig. 11. It can be found in Fig. 11 that both the R-DTC and the P-DTC have nearly the same maximum speed, which does not satisfy the theoretical analysis of Subsection V-C. This

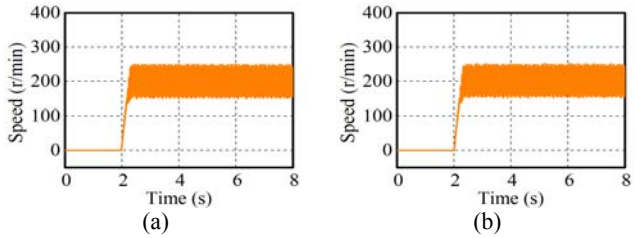

Fig. 11. Maximum speeds of coupling mode. (a) R-DTC, (b) P-DTC.

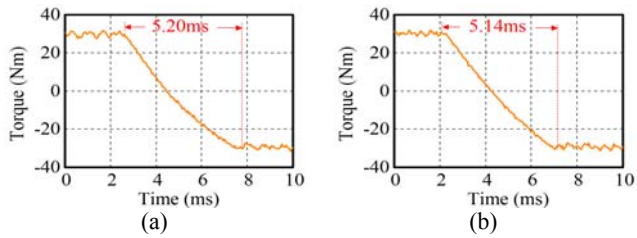

Fig. 12. Falling time of torque response of coupling mode. (a) R-DTC, (b) P-DTC.

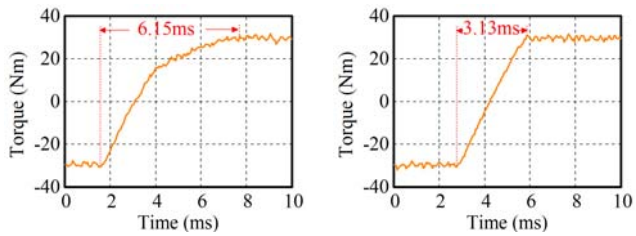

Fig. 13. Rising time of torque response of coupling mode. (a) R-DTC, (b) P-DTC.

can be explained as follows. In the coupling mode, both of the PMSMs always have the same speed, which means that they come into high-speed operation region simultaneously in this experiment. As analyzed in Subsection V-C, most of the selected switching-vectors should be active in the high-speed operation region. Therefore, the dual-PMSM drive system mostly operates in Situation-III instead of Situation-II. However, the wider speed range of the P-DTC depends on the frequent appearance of Situation-II. In other words, the speed range of the P-DTC cannot be extended in the coupling mode.

To check the torque response time in the coupling mode, Experiment-3 is carried out and its experimental conditions are set as follows: a) the dc bus voltage is set as 250 V; b) the reference speed is set as 300 r/min; and c) the total load is set as 40 Nm. The torque reference of PMSM-1 is forced to decrease from 30 Nm to -30 Nm. The corresponding torque profiles of PMSM-1 are illustrated in Fig. 12. It can be seen in Fig. 12 that both the R-DTC and the P-DTC have the same falling time for the torque response, which verifies the theoretical analysis in Subsection V-D. Then, the torque reference of PMSM-1 is forced to increase from -30 Nm to 30 Nm. The corresponding torque profiles of PMSM-1 are illustrated in Fig. 13. It can be seen in Fig. 13 that the P-DTC has a faster response ability in terms of the torque increasing,

which also verifies the theoretical analysis in Subsection V-D.

B. Independent Mode

Without special declarations, the experimental conditions in this operation mode are as same as those in the coupling mode. In the independent mode, PMSM-1 and PMSM-2 are connected with two load PMSMs, which is shown in Fig. 14.

To check the steady-state performances in the independent mode, Experiment-4 is carried out and its experimental conditions are set as follows: a) the dc bus voltage is 400 V; b) the reference speeds of PMSM-1 and PMSM-2 are set as 600 r/min and 50 r/min, respectively; c) the loads of two PMSMs are set as 20 Nm; and d) the control method is switched from the R-DTC to the P-DTC at t=4s. Fig. 15 shows experimental results from Experiment-4. It can be seen in Fig. 15 that the flux ripples of the two PMSMs remain unchanged while the torque ripple of PMSM-1 is reduced, which verifies the theoretical analysis of Subsection V-B. However, the torque ripple of PMSM-2 is nearly unchanged, which can be explained as follows. Because PMSM-1 operates in the high-speed region, most of its selected switching-vectors should be active. Meanwhile, most of the selected switching-vectors for PMSM-2 should be zero since it operates in the low-speed region. Therefore, dual-PMSM drive systems usually operate in Situation-II. As a result, the replacement of an active switching-vector to a zero vector frequently occurs in the R-DTC. However, this type of replacement is rarely found in the P-DTC. Hence, PMSM-1 and PMSM-2 have different torque ripples.

To check the maximum speed in the independent mode, Experiment-5 is carried out and its experimental conditions are set as follows: a) for safety purpose, the dc bus voltage is set as 100 V; b) the reference speeds of PMSM-1 and PMSM-2 are set as 1000 r/min and 50 r/min, respectively; and c) the loads of two PMSMs are set as 20 Nm. The corresponding experimental results are illustrated in Fig. 16. It can be found in Fig. 16 that the maximum speeds of PMSM-2 using the R-DTC and the P-DTC are 200 r/min and 280 r/min, which satisfies the theoretical analysis of Subsection V-C. This can be explained as follows. Referring to the analysis of Fig. 15, dual-PMSM drive systems usually operate in Situation-II. Since the main content of the selected switching-vector for PMSM-1 is active, the selected active switching-vectors are frequently replaced by zero vectors, which results in a reduction in the maximum speed of PMSM-1. Similarly, since the main content of the selected switching-vector for PMSM-2 is zero, the maximum speed of PMSM-2 is not affected.

To check the torque response time in the independent mode, Experiment-6 is carried out and its experimental conditions are set as follows: a) the dc bus voltage is set as 250 V; b) the reference speeds of PMSM-1 and PMSM-2 are set as 1000 r/min and 50 r/min, respectively; and c) the loads of two PMSMs are set as 20 Nm. The corresponding experimental results of PMSM-1 are illustrated in Figs. 17 and 18. They also verify the theoretical analysis in Subsection V-D.

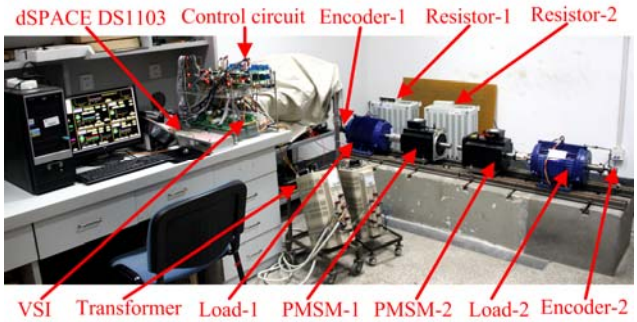

Fig. 14. Experiment platform for independent mode.

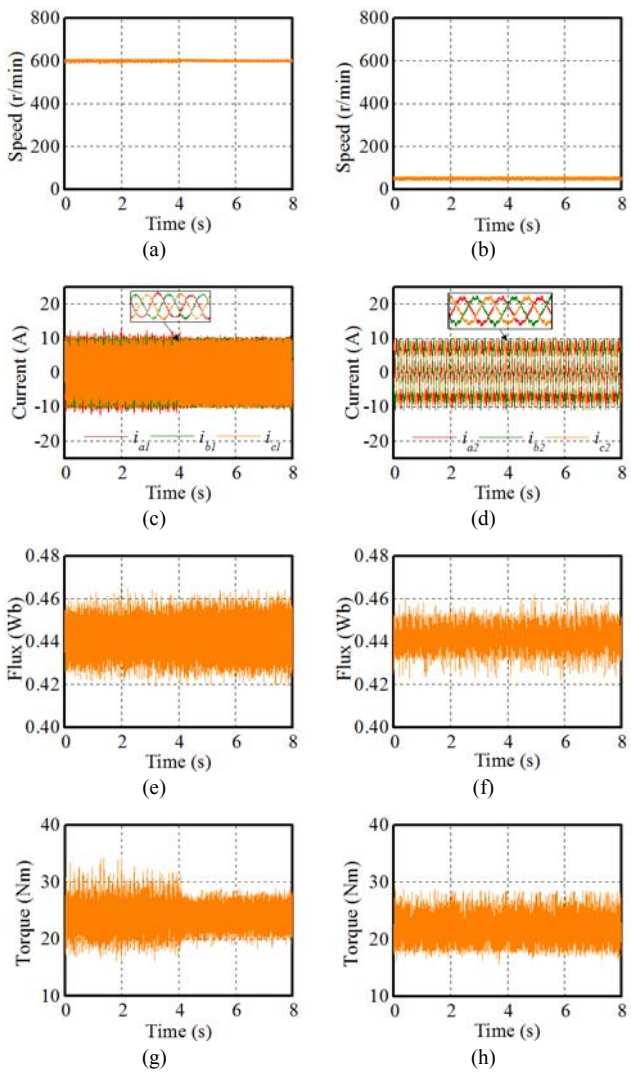

Fig. 15 Steady-state experimental results of independent mode from R-DTC to P-DTC switching at t=4 s. (a) Speed of PMSM-1, (b) speed of PMSM-2, (c) phase currents of PMSM-1, (d) phase currents of PMSM-2, (e) stator flux of PMSM-1, (f) stator flux of PMSM-2, (g) torque of PMSM-1, (h) torque of PMSM-2.

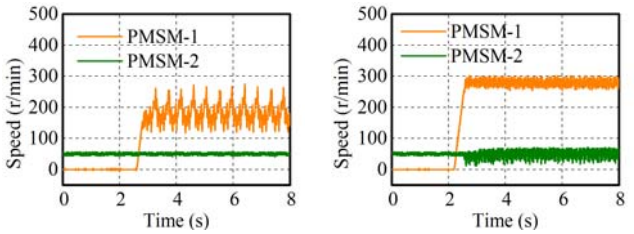

Fig. 16. Maximum speeds of independent mode. (a) R-DTC, (b) P-DTC.

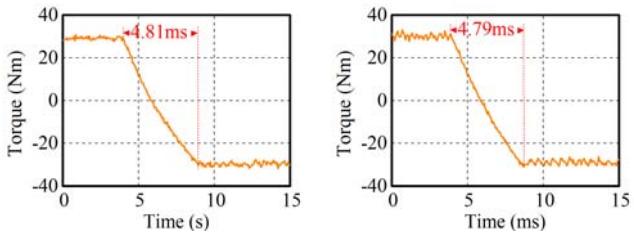

Fig. 17. Falling time of torque response of independent mode. (a) R-DTC, (b) P-DTC.

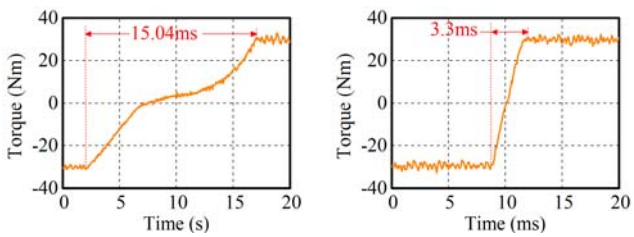

Fig. 18. Rising time of torque response of independent mode. (a) R-DTC, (b) P-DTC.

VII. CONCLUSION

In this paper, an improved DTC scheme (P-DTC) is proposed for five-leg dual-PMSM drive systems with the fault-tolerant purpose. According to the definition of the switching-vector unions, the operation of a five-leg dual-PMSM drive system is classified into three situations, and then the performances of the P-DTC are theoretically analyzed and compared with an existed DTC scheme (R-DTC) for five-leg dual-motor drive systems. According to the comparison, it is found that the P-DTC has lower torque ripples, a wider speed range and a faster torque increasing response. Experiments are carried out in both the coupling and independent modes, and the effectiveness of the P-DTC is verified by the obtained experimental results.

ACKNOWLEDGMENT

This work was supported in part by National Natural Science Foundation of China (Project: 51607038), Jiangsu Natural Science Foundation of China (Project: BK20160673), the "973 Program" of China (Project: 2013CB035603), China Postdoctoral Science Foundation (Project: 2015M581697, 2016T90401) and the Fundamental Research Funds for the Central Universities (Projrct: NJ20160043).

REFERENCES

[1] M. Cheng, W. Hua, J. Zhang, and W. Zhao, "Overview of stator-permanent magnet brushless machines," *IEEE Trans. Ind. Electron.*, Vol. 58, No. 11, pp. 5087-5101, Nov. 2011.

[2] T. M. Jahns and W. L. Soong, "Pulsating torque minimization techniques for permanent magnet AC motor drives-a review," *IEEE Trans. Ind. Electron.*, Vol. 43, No. 2, pp. 321-330, Apr. 1996.

[3] K. T. Chau, C. C. Chan, and C. H. Liu, "Overview of permanent-magnet brushless drives for electric and hybrid electric vehicles," *IEEE Trans. Ind. Electron.*, Vol. 55, No. 6, pp. 2246-2257, Jun. 2008.

[4] T. Qiu, X. Wen, and F. Zhao, "Adaptive-linear-neuron-based dead-time effects compensation scheme for PMSM drives," *IEEE Trans. Power Electron.*, Vol. 31, No. 3, pp. 2530-2538, Mar. 2016.

[5] Z. Tang, X. Li, S. Dusmez, and B. Akin, "A new V/f-based sensorless MTPA control for IPMSM drives," *IEEE Trans. Power Electron.*, Vol. 31, No. 6, pp. 4400-4415, Jun. 2016.

[6] W. Wang, J. Zhang and M. Cheng, "Fault-tolerant control of dual three-phase permanent-magnet synchronous machine drives under open phase faults," *IEEE Trans. Power Electron.*, Vol. 32, No. 3, pp. 2052-2063, Mar. 2017.

[7] W. Wang, A. Bouscayrol, and M. Cheng, "Comparison of two different traction systems for subway application using Energetic Macroscopic Representation," in *VPPC*, pp. 984-989, 2012.

[8] J. O. Estima and A. J. M. Cardoso, "A fault-tolerant permanent magnet synchronous motor drive with integrated voltage source inverter open-circuit faults diagnosis," in *Proc. EPE*, pp. 1-10, 2011.

[9] X. Pei, S. Nie, and Y. Kang, "Switch short-circuit fault diagnosis and remedial strategy for full-bridge DC–DC converters," *IEEE Trans. Power Electron.*, Vol. 30, No. 2, pp. 996-1004, Feb. 2015.

[10] B. Ji, X. Song, W. Cao, V. Pickert, Y. Hu, J. W. Mackersie, and G. Pierce, "In situ diagnostics and prognositics of solder fatigue in IGBT modules for electric vehicle drives," *IEEE Trans. Power Electron.*, Vol. 30, No. 3, pp. 1535-1543, Mar. 2015.

[11] J. Choi, S. Kim, S. Y. Dong, and K. Kim, "A diagnostic method of simultaneous open-switch faults in inverter-fed linear induction motor drive for reliability enhancement," *IEEE Trans. Ind. Electron.*, Vol. 62, No. 7, pp. 4065-4077, Jul. 2015.

[12] B. Gou, X. Ge, S. Wang, X. Feng, J. B. Kuo, and T. G. Habetler, "An open-switch fault diagnosis method for single-phase PWM rectifier using a model-based approach in high-speed railway electrical traction drive system," *IEEE Trans. Power Electron.*, Vol. 31, No. 5, pp. 3816-3826, May 2016.

[13] F. Wu and J. Zhao, "A real-time multiple open-circuit fault diagnosis method in voltage-source-inverter fed vector controlled drives," *IEEE Trans. Power Electron.*, Vol. 31, No. 2, pp. 1425-1437, Feb. 2016.

[14] B. Mirafzal, "Survey of fault-tolerance techniques for three-phase voltage source inverters," *IEEE Trans. Ind. Electron.*, Vol. 61, No. 10, pp. 5192-5202, Oct. 2014.

[15] T. Kamel, Y. Biletskiy and L. Chang, "Real-time diagnosis

for open-circuited and unbalance faults in electronic converters connected to residential wind systems," *IEEE Trans. Ind. Electron.*, Vol. 63, No. 3, pp. 1781-1792, Mar. 2016.
[16] S. Nie, X. Pei, Y. Chen, and Y. Kang, "Fault diagnosis of PWM DC-DC converters based on magnetic component voltages equation," *IEEE Trans. Power Electron.*, Vol. 29, No. 9, pp. 4978-4988, Sep. 2014.
[17] Q. An, L. Sun and L. Z. Sun, "Current residual vector-based open-switch fault diagnosis of inverters in PMSM drive systems," *IEEE Trans. Power Electron.*, Vol. 30, No. 5, pp. 2814-2827, May 2015.
[18] W. Wang, M. Cheng, B. Zhang, Y. Zhu, and S. Ding, "A fault-tolerant permanent-magnet traction module for subway applications," *IEEE Trans. Power Electron.*, Vol. 29, No. 4, pp. 1646-1658, Apr. 2014.
[19] K. Oka, Y. Nozawa, and K. Matsuse, "Improved method of voltage utility factor for PWM control method of five-leg inverter," in *PESC*, pp. 1-5, 2006.
[20] M. Jones, S. N. Vukosavic, D. Dujic, E. Levi, and P. Wright, "Five-leg inverter PWM technique for reduced switch count two-motor constant power applications," *IET Electr. Power Appl.*, Vol. 2, No. 5, pp. 275-287, Sep. 2008.
[21] M. Hizume, S. Yokomizo, and K. Matsuse, "Independent vector control of parallel connected two induction motors by a five-leg inverter," in *EPE*, pp. 1-7, 2003.
[22] W. Wang, J. Zhang, and M. Cheng, "A dual-level hysteresis current control for one five-leg VSI to control two PMSMs," *IEEE Trans. Power Electron.*, Vol. 32, No. 1, pp. 804-814, Jan. 2017.
[23] P. Delarue, A. Bouscayrol, and E. Semail, "Generic control method of multi-leg voltage-source-converters for fast practical implementation," *IEEE Trans. Power Electron.*, Vol. 18, No. 2, pp. 517-526, Mar. 2003.
[24] C. S. Lim, E. Levi, M. Jones, N. A. Rahim, and W. P. Hew, "A comparative study of synchronous current control schemes based on FCS-MPC and PI-PWM for a two-motor three-phase drive," *IEEE Trans. Ind. Electron.*, Vol. 61, No. 8, pp. 3867-3878, Aug. 2014.
[25] C. S. Lim, N. A. Rahim, W. P. Hew, and E. Levi, "Model predictive control of a two-motor drive with five-leg-inverter supply," *IEEE Trans. Ind. Electron.*, Vol. 60, No. 1, pp. 54-65, Jan. 2013.
[26] A. Khodadoost and A. Radan, "Novel comparative study between SVM, DTC and DTC-SVM in five-leg inverter to drive two motors independently," in *Proc. PEDSTC*, Tehran, Iran, 2013, pp. 1-7.
[27] G. S. Buja and M. P. Kazmierkowski, "Direct torque control of PWM inverter-fed AC motors – A survey," *IEEE Trans. Ind. Electron.*, Vol. 51, No. 4, pp. 744-757, Aug. 2004.
[28] L. Zhong, M. F. Rahman, W. Y. Hu, and K. W. Lim, "Analysis of direct torque control in permanent magnet synchronous motor drives," *IEEE Trans. Power Electron.*, Vol. 12, No. 3, pp. 528-536, May 1997.

Wei Wang was born in Jiangsu, China. He received his B.S. degree in Electrical Engineering from the Nanjing University of Science and Technology, Nanjing, China, in 2008; and his Ph.D. degree in Electrical Engineering from Southeast University, Nanjing, China, in 2014. Since 2014, he has been with Southeast University, where he is presently working as a Lecturer in the School of Electrical Engineering. From October 2011 to October 2012, he received a scholarship from the China Scholarship Council and was a joint Ph.D. student at the Lille University of Science and Technology, Lille, France. He is the author or coauthor of more than 30 technical papers. His current research interests include motor drives and traction systems for rail transit.

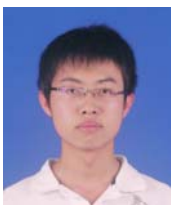

Jinghao Zhang was born in Gansu, China. He received his B.S. degree in Electrical Engineering from the Nanjing University of Science and Technology, Nanjing, China, in 2014. He is presently working towards his M.S. degree in Electrical Engineering at Southeast University, Nanjing, China. His current research interests include electrical machine drives and traction systems for rail transit.

Ming Cheng received his B.S. and M.S. degrees from the Department of Electrical Engineering, Southeast University, Nanjing, China, in 1982 and 1987, respectively; and his Ph.D. degree from the Department of Electrical and Electronic Engineering, University of Hong Kong, Hong Kong, China, in 2001. Since 1987, he has been with Southeast University, where he is presently working as a Distinguished Professor in the School of Electrical Engineering and as the Director of the Research Center for Wind Power Generation. From January 2011 to April 2011, he was a Visiting Professor with the Wisconsin Electric Machine and Power Electronics Consortium, University of Wisconsin, Madison, WI, USA. His current teaching and research interests include electrical machines, motor drives for EVs, and renewable energy generation. He has authored or co-authored more than 300 technical papers and four books, and is the holder of 70 patents in these areas. Prof. Cheng is a Fellow of the Institution of Engineering and Technology. He has served as the Chair and an Organizing Committee Member for many international conferences. He was a Distinguished Lecturer of the IEEE Industry Applications Society for 2015/2016.

Ruiwu Cao received his B.S. degree from the Yancheng Institute of Technology, Yancheng, China, in 2004; and his M.S. and Ph.D. degrees in Electrical Engineering from Southeast University, Nanjing, China, in 2007 and 2013, respectively. From August 2010 to November 2011, he was a joint Ph.D. student with the College of Electrical and Computer Science, University of Michigan, Dearborn, MI, USA, funded by the China Scholarship Council. Since 2013, he has been with the Nanjing University of Aeronautics and Astronautics, Nanjing, China, where he is presently working as an Associate Professor in the Department of Electrical Engineering. His current teaching and research interests include linear motors for rail transit, electromagnetic launch systems, motor drives for electric vehicles and renewable energy generation.